PCCP

Accepted Manuscript

ROYAL SOCIETY OF CHEMISTRY

www.rsc.org/pccp

Journal Name

ARTICLE TYPE

Cite this: DOI: 10.1039/xxxxxxxxxx

Ab-initio Energy Loss Spectra of Si and Ge Nanowires

Maurizia Palummo,*[a] Conor Hogan[a,b] and Stefano Ossicini[c]

Received Date
Accepted Date

DOI: 10.1039/xxxxxxxxxx

www.rsc.org/journalname

We report an *ab initio* investigation of fast electron energy-loss probability in silicon and germanium nanowires. Computed energy loss spectra are characterized by a strong enhancement of the direct interband transitions peak at low energy, in good agreement with experimental data. Our calculations predict an important diameter dependence of the bulk volume plasmon peak for very thin wires which is consistent with the blue shift observed experimentally in thicker wires.

1 Introduction

Semiconductor nanowires (NWs) have attracted wide interest in recent years, thanks to their potential use in a variety of nanoelectronic and photonic devices. Silicon and germanium NWs offer particularly good compatibility with established silicon-based microelectronics and their use in appliances, ranging from bipolar and field-effect transistors to nanoscale sensors and nonvolatile memory devices, has been demonstrated.[1–6]

Si and Ge NWs are currently grown through various synthetic methods, bottom-up techniques or top-down approaches. The most used methodology is the vapor-liquid-solid (VLS) mechanism, in which a catalytic nanoparticle, normally Au, is used to promote the decomposition of an appropriate gaseous precursor. The obtained wires have single crystal nature and grow along well-defined crystalline orientation. The diameter of the NWs depend on the orientation: the smallest (a few nanometers) are obtained, usually, for the $\langle 110 \rangle$ direction; the largest for the $\langle 111 \rangle$ direction; and intermediate ones, about 10 nm, for the $\langle 112 \rangle$ direction.[5–8] Many experimental[9–12] and theoretical[13–19] studies have been carried out on these materials. In spite of the progress made, significant uncertainty remains concerning their fundamental physical properties, in part due to the difficulty in correlating the experimental observations with the electronic properties, and due to the use of simplified models in theoretical calculations. Regarding the latter, studies at both the semi-empirical and *ab initio* levels[20–25] have aimed to interpret the electronic and optical data in the visible-UV region, and succeeded to demonstrate the important role played by excitons in the optical properties of these one-dimensional systems.[23,24]

Among the experimental techniques, electron energy loss spectroscopy combined with scanning transmission microscopy (EELS-STEM) has been developed into a powerful means to study electronic excitations in nanostructures. Interesting and particular features have been observed in the EELS spectra of semiconductor NWs (including Si and Ge NWs) as well as in C, BN, and WS_2 nanotubes,[26–33] and are believed to derive from the reduced dimensionality of these systems. Nevertheless, few theoretical studies have addressed the interpretation of EELS spectra of nanostructures. Most of these have been based on the continuum dielectric theory, which neglects the quantum confinement effects on the electronic structure, and as such, can only be considered a reasonable approach for large nanostructures. Only one theoretical study, about zero and one-dimensional Si nanostructures, is present in the literature which calculates EELS spectra based on atomistic calculations, albeit within the parametrized tight-binding approach.[34] It is noticeable that this work fails to reproduce the low energy peak observed in experiments of very thin Si nanostructures. The aim of the present work is to provide a first-principles theoretical analysis of the dynamical dielectric response and EELS spectra for Si and Ge NWs. The main goal is to elucidate, using the available EELS measurements the connection between the NW structural parameters and the observed spectra of these nanomaterials.

2 Theoretical Approach

2.1 *Ab-initio* response function

Density-functional theory within the local-density approximation (DFT-LDA) calculations of Si and Ge wires were carried out by means of a plane-wave code (ABINIT[35]) and norm-conserving pseudopotentials.[36] Kinetic energy cutoffs of 20 and 30 Ry, for Si and Ge NWs respectively, have been used. A vacuum region of 1.5 nm has been used to simulate the isolated wires. A one-dimensional $8 \times 1 \times 1$ k-grid is used for self-consistent DFT simulations, while the sampling is increased to a $16 \times 1 \times 1$ grid for the

[a] *Dipartimento di Fisica e European Theoretical Spectroscopy Facility (ETSF), Universitá degli Studi di Roma "Tor Vergata", Via della Ricerca Scientifica 1, 00133 Roma, Italy.*
[b] *Istituto di Struttura della Materia, Consiglio Nazionale delle Ricerche (CNR-ISM), Via Fosso del Cavaliere 100, 00133 Roma, Italy.*
[c] *Dipartimento di Scienze e Metodi dell'Ingegneria, Universitá di Modena e Reggio Emilia, via Amendola 2 Pad. Morselli, I-42100 Reggio Emilia, Italy.*
* *Corresponding author. E-mail: maurizia.palummo@roma2.infn.it*

non-self-consistent runs needed to calculate the dielectric functions. Convergence of the results has been carefully checked with respect to the kinetic energy cut-off, the **k**-point sampling, and the vacuum size within the simulation cell. All the wires under study were oriented along the [100] direction. See refs.[23,25,37] for further details of the NW geometries and calculation methods.

Surface dangling bonds were saturated with hydrogen atoms in order to eliminate states within the electronic gaps. The geometrical structure of the relaxed ground-state configuration of each wire has been obtained by solving self-consistently the one-particle Kohn-Sham equations (KS),[38,39] and the obtained KS eigenvectors and eigenvalues were used in the calculation of the full dielectric matrix.[40] This was done within the linear response theory using the random phase approximation (RPA) and including the so-called local-field effects (LFE).[41]

In this approach—usually referred as the time-dependent Hartree-Fock method—the density response function is the crucial quantity to be calculated. It connects the induced electron density to the external potential and satisfies the integral equation: $\chi = \chi^0 + \chi^0 v \chi$. Here all the correlation effects are neglected, whereas the LFE resulting from the microscopic part of the density variation of the Hartree potential are retained. For the nanostructures under study (or any 1-D system, in fact), it has already been shown that the inclusion of LFE is essential to describe the experimentally observed "depolarization effect", in which the component of the dielectric tensor perpendicular to the wire axis (the radial component) is strongly depressed with respect to the parallel component.[23,25,42]

The macroscopic dielectric function is obtained as

$$\varepsilon_M(\omega) = \lim_{q\to 0} \frac{1}{[1+v(q)\chi(q,\omega)]_{\mathrm{G=G'=0}}}. \qquad (1)$$

In principle, for a more accurate description of the dielectric function, both self-energy and excitonic effects should be included in the calculation. However, computation of EELS spectra requires a wide energy range, which would imply treating a huge number of transitions at this level of theory, hence making the calculation intractable or at least very cumbersome. It has been shown in previous studies that, in Si and Ge [100]-oriented NWs, these effects actually compensate quite well.[23,25] Furthermore, in the EELS spectra of bulk semiconducting compounds, excitonic effects play a minor role with respect to the local-field effects.[43]

2.2 Simulation of EELS

To calculate the energy loss probability we follow the approach proposed in refs.[44–46], which describes electrons impinging upon a nanowire at a given impact parameter b, in a non-penetrating geometry. Under the assumption that the thickness of the nano-object is a much more important parameter than its actual geometry, the loss probability for the NW can be calculated from the following expression for an anisotropic slab:[46] $P(\omega,b) = \int_0^\infty dk C_k(\omega,b)\mathrm{Im}\gamma_K(\omega)$, where K is the modulus of the transferred momentum, $C_K(\omega) \simeq e^{-Kb}$ is a kinematic factor and

$$\gamma_K(\omega) = -\frac{[1-\varepsilon_\parallel\varepsilon_\perp]\sinh(Kd/\sqrt{\lambda})}{[1+\sqrt{\varepsilon_\parallel\varepsilon_\perp}]^2 e^{Kd/\sqrt{\lambda}} - [1-\sqrt{\varepsilon_\parallel\varepsilon_\perp}]^2 e^{-Kd/\sqrt{\lambda}}}. \qquad (2)$$

Here $\varepsilon_\perp$ ($\varepsilon_\parallel$) is the radial (axial) component of the dielectric function of the isolated nanowire, $\lambda = \varepsilon_\perp/\varepsilon_\parallel$, and d is the NW diameter. Finally, since the studied NWs are very thin, and the transferred momenta (available from the experiments) are very small, $Kd \ll 1$ and $\gamma_K(\omega)$ can be reduced to $\frac{Kd}{4}[\frac{-1}{\varepsilon_\perp(\omega)} + \varepsilon_\parallel(\omega)]$. Hence, the loss resonances occur at the maxima of $\mathrm{Im}[\varepsilon_\parallel(\omega)]$ and of $\mathrm{Im}[\frac{1}{\varepsilon_\perp(\omega)}]$.

It is important to point out that, within a repeated cell approach as used here, the output of the simulation is the dielectric response of a periodic *lattice* or supercell of parallel NWs. What is required for the EELS calculation (Equation 2), however, is the knowledge of the dielectric response of the *isolated* nanostructure. As stressed by several authors,[47,48] depolarization effects related to the long-range electrostatic interactions between NWs in different cells have to be eliminated, whereas the so-called "surface depolarization" effects, arising from the solid-vacuum interface of an isolated NW, must remain in the calculation.

The axial ($\alpha_\parallel$) and radial ($\alpha_\perp$) components of the polarizability of the isolated NW can be extracted from the corresponding components of the dielectric response of the NW lattice, as obtained in a supercell (SC) calculation ($\varepsilon_\parallel^{\mathrm{SC}}$, $\varepsilon_\perp^{\mathrm{SC}}$) in the following way. For the axial component, the relation is straightforward: $\alpha_\parallel = (\Omega^{\mathrm{SC}}/4\pi)(\varepsilon_\parallel^{\mathrm{SC}} - 1)$, where Ω^{SC} is the supercell area in the plane perpendicular to the wire growth direction. For the radial component, we use a 2-D Clausius-Mossotti relation[47,48] in order to eliminate the depolarization effects arising from the NW images in the other cells: $\alpha_\perp = (\Omega^{\mathrm{SC}}/2\pi)(\varepsilon_\perp^{\mathrm{SC}} - 1)/(\varepsilon_\perp^{\mathrm{SC}} + 1)$. Once these long-range effects have been removed, the effective dielectric function of the truly isolated nanowire, both in the axial and radial direction, is obtained from:[48,49]

$$\varepsilon_{\parallel,\perp} = 1 + \frac{4\pi}{\Omega^{\mathrm{NW}}}\alpha_{\parallel,\perp} \qquad (3)$$

where Ω^{NW} is the cross sectional area of the *nanowire*, and $\varepsilon_{\parallel,\perp}$ still fully contain the effects of (local) surface depolarization and quantum confinement.

3 Results and Discussion

In Figures 1 and 2 we report both the axial and radial components of the dielectric function of isolated Si and Ge NWs with different diameters, extracted from the supercell data using Eq. 3. The different behaviour of the axial and radial components is immediately evident. While a clear reduction of the static axial screening is observed while decreasing the NW diameter, the radial component Re $[\varepsilon_\perp(0)]$ remains almost constant (see top panels). The different behaviour of the two components is evident also for the imaginary parts (see bottom panels). A blue shift of Im $[\varepsilon_\parallel(\omega)]$ is observed due to the quantum confinement effect, which is stronger for Ge than for Si NWs, as must be expected because of the larger exciton Bohr radius in Ge. In contrast, the depolarization effects ensure that the radial components are greatly reduced

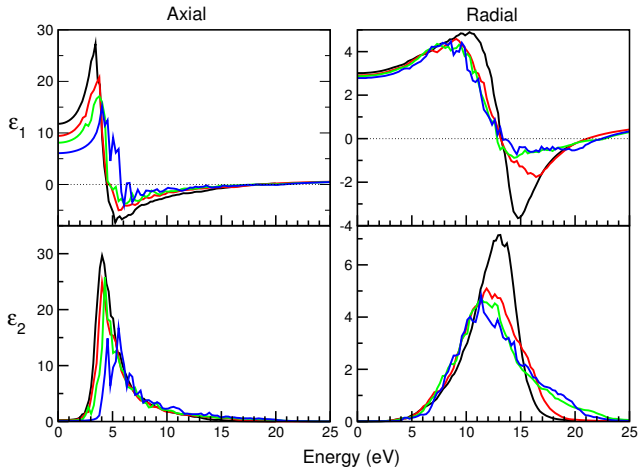

Fig. 1 Si[100] NWs. Real (top panels) and Imaginary part (bottom panels) of the axial (left) and radial (right) components of the dielectric function for wires of different size d. Black: 1.9 nm; red: 1.4 nm; green: 1.0 nm; blue: 0.63 nm.

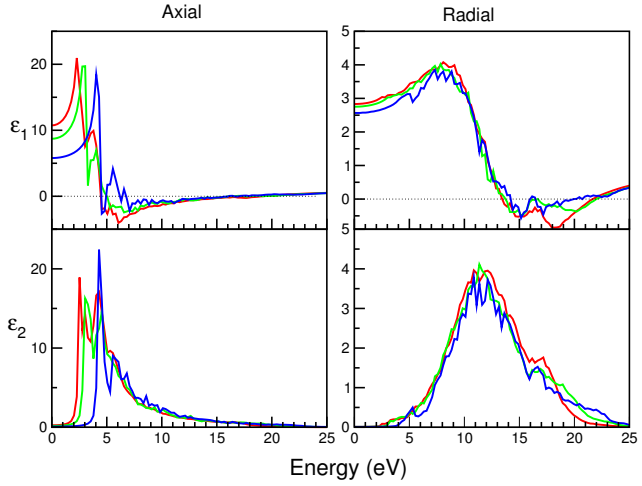

Fig. 2 Ge[100] NWs. Real (top panels) and Imaginary part (bottom panels) of the axial (left) and radial (right) components of the dielectric function for wires of different size d. Red: 1.42 nm; green: 1.05 nm; blue: 0.69 nm.

in intensity, remaining close to zero below the high energy peak occurring somewhat independently of the NW size around 12 eV. In ref.[50] it was shown how the classical effective medium theory is able to explain this feature. For any 1-D isolated nano-object Im $[\varepsilon_\perp(\omega)]$ will never tend to the absorption of the bulk, but will instead remain positioned at the maximum of Im $[\frac{1}{\varepsilon_{\rm bulk}+1}]$, which coincides with the surface-plasmon peak position of the material, which for Si and Ge is located around 12.8 eV and 11 eV respectively.

The absorptive parts (both parallel and radial components) of the dielectric functions were found to satisfy the bulk f-sum rule, almost independently of the NW size. This suggests that the electron density inside the wires is not very different from the bulk case. Furthermore, the energy (i.e. the longitudinal frequency ω_L) where the corresponding real components become zero is

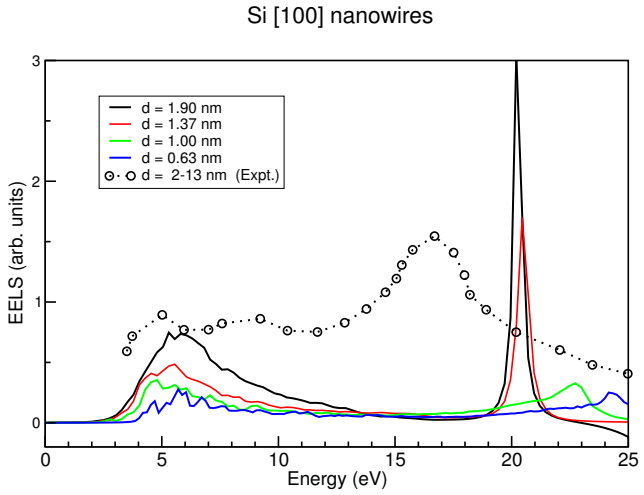

Fig. 3 Comparison between theoretical EELS spectra for Si NWs of different diameter with the experimental TEM-EELS data.[29]

strongly blue-shifted with respect to the plasma frequency, $\omega_{\rm pl}$, as the nanowire diameter is decreased. In fact, considering a simple Lorentz model, for a material with an electronic gap ω_0, the longitudinal frequency results to be $\omega_L^2 = \omega_0^2 + \omega_{\rm pl}^2$. In this way the longitudinal frequencies are blue-shifted when the gap increases: this is due to quantum-confinement effects for the axial components, and to a combination of quantum-confinement and depolarization effects, for the radial ones.

Computed energy loss spectra for several Si and Ge NWs are compared with available experimental TEM-EELS data, in Figs. 3 and 4. It is evident that, in contrast to tight-binding results,[34] our *ab initio* results clearly reproduce the low energy peaks observed in both materials. These low-energy features, which are associated with interband transitions, are strongly enhanced as the NW diameter is increased in both cases. This finding is consistent with the results obtained by Reed *et al.*[27] and Zabala *et al.*[51] who showed, using a multipolar dielectric theory, that when the transferred momentum is small the low energy part of the EELS spectra of NWs with diameters of few nanometers is essentially proportional to Im $\varepsilon_{\rm bulk}$. In contrast to those studies, however, we have here fully taken into account the effects of electronic structure, quantum confinement and depolarization arising from the reduced dimensionality. For Si NWs, the absence of a peak around 7–9 eV in the theoretical spectra, which is instead present in the experimental curve of Fig. 3, confirms its origin due to the Si/SiO_2 interface plasmon excitation.[29] As the NW size decreases, a clear blue-shift of the theoretical high-energy EELS peak—deriving from the maximum of Im$[\frac{-1}{\varepsilon_\perp(\omega)}]$, as explained above—is evident for both Si and Ge.

The apparent disagreement with the experimental curves in Figs. 3 and 4 is due to the fact that the diameters of our computed NWs are much smaller than those used in the experiments. To better demonstrate this interpretation, in Fig. 5 we report the computed energetic positions of the high energy EELS peak as a function of NW size, together with experimental measurements ascribed to the volume plasmon (at $\omega_{\rm pl}$) as reported for Si[27] and

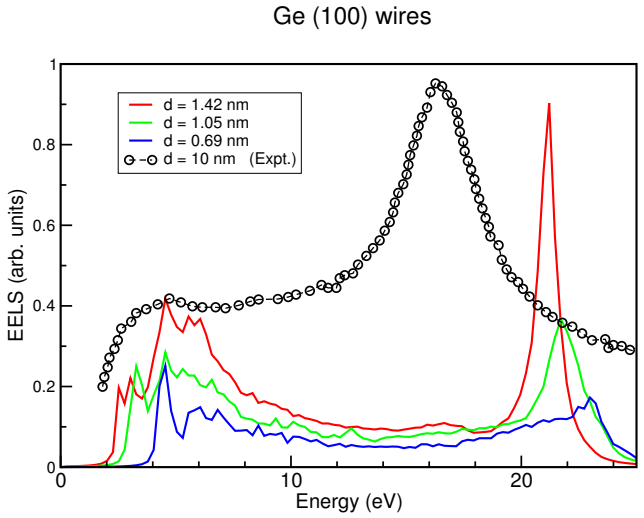

Fig. 4 Comparison between the theoretical EELS spectra for Ge NWs of different diameter and the experimental TEM-EELS data.[28]

Ge[28] NWs of larger diameters. For both materials we fitted the *experimental* data with the scaling law $\omega_{\rm pl} + C/d^{\beta}$, where d is the NW diameter. For consistency, we fix the exponents β to the values previously obtained by us[52] in a similar fit of the electronic gaps of the same nanowires. (It is notable that the scaling exponent for Ge NWs is very close to the best fitbest fit value ($\beta = 1.2$) reported in ref.[28].) The two corresponding curves are reported in Fig. 5 (solid lines). In both cases (and as noted in ref.[28] for Ge) we obtain better fits to the ensemble of experimental and theoretical data with these exponents than what is predicted (dashed lines) from a simple particle-in-a-box model with $\beta = 2$, often used to explain confinement in zero-dimensional nanoparticles.[53,54]

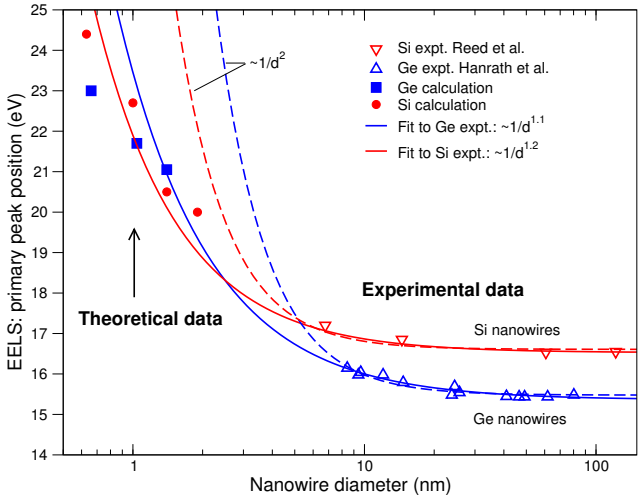

Fig. 5 Plasmon peak position in Si (red) and Ge (blue) NWs for varying diameters. Calculated results are indicated by circles (Si) and squares (Ge), and experimental data are shown by down triangles (Si, ref.[27]) and up triangles (Ge, ref.[28]). Lines are fits to the experimental data, for selected exponents (see text).

4 Conclusions

In conclusion, we have investigated by first-principle methods the energy loss spectra of Si and Ge NWs. The presence and strong enhancement of a direct interband transition peak, in agreement with experiments, has been found. Moreover a clear size dependence of the bulk volume plasmon peak position has been obtained as due to a proper description of electronic structure, quantum confinement and surface depolarization.

5 Acknowledgments

We acknowledge the CINECA award under the ISCRA initiative, for the availability of high performance computing resources and support.

References

1 Y. Cui and C. M. Lieber, *Science*, 2001, **291**, 851.
2 Y. Cui, Z. Zhong, D. Wang and C. M. Lieber, *Nano Lett.*, 2003, **3**, 149–152.
3 J. Hahm and C. M. Lieber, *Nano Lett.*, 2004, **4**, 51.
4 O. Bisi, S. Ossicini and L. Pavesi, *Surf. Science Rep.*, 2000, **38**, 1–126.
5 R. Rurali, *Rev. Mod. Phys.*, 2010, **82**, 427.
6 M. Amato, M. Palummo, R. Rurali and S. Ossicini, *Chem. Rev.*, 2014, **114**, 1371–1412.
7 Y. Wu, Y. Cui, L. Huyn, C. Barrelet, D. Bell and C. Lieber, *Nano Letters*, 2004, **4**, 433.
8 C. O'Regan, S. Biswas, N. Petkov and J. D. Holmes, *J. Mater. Chem B*, 2014, **14**, 2.
9 D. D. D. Ma, C. S. Lee, F. C. K. Au, S. Y. Tong and S. T. Lee, *Science*, 2003, **299**, 1874.
10 T. Hanrath and B. Korgel, *Small*, 2005, **1**, 717.
11 K. Q. Peng, X. Wang, L. Li, Y. Hu and S. Lee, *Nanotoday*, 2013, **8**, 75.
12 S. Biswas, C. O. Regan, N. Petkov, M. A. Morris and J. D. Holmes, *Nano Lett.*, 2012, **12**, 5654–5663.
13 J. D. Holmes, K. P. Johnston, R. C. Doty and B. A.Korgel, *Science*, 2000, **286**, 1471.
14 R. Pekoz and J.-Y. Raty, *Phys. Rev. B*, 2009, **80**, 155432.
15 P. Logan and X. Peng, *Phys. Rev. B*, 2009, **80**, 115322.
16 M.-F. Ng, M. Sullivan, S. Tong and P. Wu, *Nano Lett.*, 2011, **11**, 4794.
17 H. Peelaers, B. Partoens, M. Giantomassi, T. Rangel, E. Goossens, G. M. Rignanese, X. Gonze and F. Peeters, *Phys. Rev. B*, 2011, **83**, 045306.
18 L. Zhang, J.-W. Luo, A. Franceschetti and A. Zunger, *Phys. Rev. B*, 2011, **84**, 075404.
19 Y. Ping, D. Rocca, D. Y. Lu and G. Galli, *Phys. Rev. B*, 2012, **85**, 035316.
20 Y. Niquet, A. Lherbier, N. Quang, M. Fernández-Serra, X. Blase and C. Delerue, *Phys Rev B*, 2006, **73**, 165319.
21 R. Rurali and N. Lorente, *Phys. Rev. Lett.*, 2005, **94**, 026805.
22 X. Zhao, C. Wei, L. Yang and M. Chou, *Phys. Rev. Lett.*, 2004, **92**, 236805.

23 M. Bruno, M. Palummo, A. Marini, R. Del Sole and S. Ossicini, *Phys. Rev. Lett.*, 2007, **98**, 036807.

24 L. Yang, C. Spataru, S. Louie and M. Chou, *Phys. Rev. B*, 2007, **75**, 201304.

25 M. Bruno, M. Palummo, M. Marini, R. Del Sole, V. Olevano, A. Kholod and S. Ossicini, *Phys. Rev. B*, 2005, **72**, 153310.

26 R. Sassaki, F. Galembeck and O. Teschke, *Appl. Phys. Lett.*, 1996, **69**, 206.

27 R. Reed, J. M. Chen, N. MacDonald, J. Silcox and G. Bertsch, *Phys. Rev. B*, 1999, **60**, 5641.

28 T. Hanrath and B. Korgel, *Nano Lett.*, 2004, **4**, 1455.

29 J. Kikkawa, S. Takeda, Y. Sato and M. Terauchi, *Phys. Rev. B*, 2007, **75**, 245317.

30 J. Hyun, , M. Levendorf, M. Blood-Forsythe, J. Park and D. A. Muller, *Phys. Rev. B*, 2010, **81**, 165403.

31 O. Stéphan, D. Taverna, M. Kociak, K. Suenaga, L. Henrard and C. Colliex, *Phys. Rev. B*, 2002, **66**, 155422.

32 R. Arenal, O. Stéphan, M. Kociak, D. Taverna, A. Loiseau and C. Colliex, *Phys. Rev. Lett.*, 2005, **95**, 127601.

33 B. Swain, B. Swain and N. Hwang, *J. Appl. Phys.*, 2010, **108**, 073709.

34 C. Delerue, M. Lannoo and G. Allan, *Phys. Rev. B*, 1997, **56**, 15306.

35 X. Gonze, B. Amadon, P.-M. Anglade, J.-M. Beuken, F. Bottin, P. Boulanger, F. Bruneval, D. Caliste, R. Caracas, M. Côté, T. Deutsch, L. Genovese, P. Ghosez, M. Giantomassi, S. Goedecker, D. Hamann, P. Hermet, F. Jollet, G. Jomard, S. Leroux, M. Mancini, S. Mazevet, M. Oliveira, G. Onida, Y. Pouillon, T. Rangel, G.-M. Rignanese, D. Sangalli, R. Shaltaf, M. Torrent, M. Verstraete, G. Zerah and J. Zwanziger, *Comp. Phys. Comm.*, 2009, **180**, 2582.

36 N. Troullier and J. L. Martins, *Phys Rev. B*, 1991, **43**, 1993.

37 M. Bruno, M. Palummo, S. Ossicini and R. Del Sole, *Surf. Sci.*, 2007, **601**, 2707.

38 P. Hohenberg and W. W. Kohn, *Phys. Rev.*, 1964, **136**, B864.

39 W. Kohn and L. Sham, *Phys. Rev.*, 1965, **140**, A1113.

40 A. Marini, C. Hogan, M. Grüning and D. Varsano, *Comp. Phys. Comm.*, 2009, **180**, 1392–1403.

41 G. Onida, L. Reining and A. Rubio, *Rev. Mod. Phys.*, 2002, **74**, 601.

42 A. G. Marinopoulos, L. Reining and A. Rubio, *Phys. Rev. Lett.*, 2003, **91**, 046402.

43 V. Olevano and L. Reining, *Phys. Rev. Lett.*, 2001, **86**, 5962.

44 P. E. Batson, *Ultramicroscopy*, 1983, **11**, 299.

45 P. Lambin, A. A. Lucas and J. P. Vigneron, *Phys. Rev. B*, 1992, **46**, 1794.

46 M. Kociak, O. Stéphan, L. Henrard, V. Charbois, A. Rothschild, R. Tenne and C. Colliex, *Phys. Rev. Lett.*, 2001, **87**, 075501.

47 L. Wirtz, M. Lazzeri, F. Mauri and A. Rubio, *Phys. Rev. B*, 2005, **71**, 241402.

48 B. Kozinsky and N. Marzari, *Phys. Rev. Lett.*, 2006, **96**, 166801.

49 F. Trani, D. Ninno and G. Iadonisi, *Phys. Rev. B*, 2007, **75**, 033312.

50 F. Sottile, F. Bruneval, A. Marinopoulos, L. Dash, S. Botti, V. Olevano, N. Vast, A. Rubio and L. Reining, *Int. J. Quant. Chem.*, 2005, **102**, 684.

51 N. Zabala, E. Ogando, A. Rivacoba and F. García de Abajo, *Phys. Rev. B*, 2001, **64**, 205410.

52 M. Palummo, M. Amato and S. Ossicini, *Phys. Rev. B*, 2010, **82**, 073305.

53 M. M. Mitome, Y. Yamazaki, H. Takagi and T. Nakagiri, *J. Appl. Phys.*, 1992, **72**, 812.

54 Y. Wang, J. Kim, G. Kim and K. Kim, *Appl. Phys. Lett.*, 2006, **88**, 143106.